ELSEVIER

Biophysical Chemistry 130 (2007) 76–87

Biophysical Chemistry

http://www.elsevier.com/locate/biophyschem

Conformational changes in human integrin $\alpha_{IIb}\beta_3$ after platelet activation, monitored by FRET

Ana Coutinho [1], Carolina García, José González-Rodríguez, M. Pilar Lillo *

Departamento de Biofísica, Instituto de Química Física "Rocasolano". Consejo Superior de Investigaciones Científicas, Serrano 119. 28006 Madrid, Spain

Received 12 June 2007; received in revised form 25 July 2007; accepted 26 July 2007
Available online 8 August 2007

Abstract

Integrin $\alpha_{IIb}\beta_3$, an abundant heterodimeric receptor at the surface of blood platelets, binds adhesive proteins after platelet activation and plays a primary role in haemostasis. In solution, it has been observed mainly in two conformations: the bent and the extended forms. Based on X-ray crystallography, electron microscopy and immunochemical observations of full-length integrin ectodomains and intact integrins, it has been agreed that unactivated integrins are in the bent conformation, both isolated in solution and in living cells. However, consensus is yet to emerge on the bent or extended conformation of activated integrins and on their mechanism of activation (the switchblade, the deadbolt and the S–S reduction models), which require further experimental tests at the cell level to become established facts.

Here, we tested the proposed structural rearrangements undergone by integrin $\alpha_{IIb}\beta_3$ after cell activation, by using Förster-type fluorescence resonance energy transfer (FRET) and attached fluorescent labels to Fab fragments of monoclonal antibodies directed to the βA domain of the β_3 subunit (donor, Alexa488-P97 Fab) and to the Calf-2 domain of the α_{IIb} subunit (acceptor, Cy3-M3 Fab or Cy3-M10 Fab). The FRET efficiencies observed after ADP or TRAP platelet activation changed less than 20% from the resting values, showing that the distance between the labeled Fab fragments changes only modestly after platelet activation by physiological agonists. This observation is consistent with a conformational model of the activated integrin in the cell less extended than in the switchblade model.

Keywords: Fibrinogen receptor; Human integrin; Platelet activation; Antibody labelling; Conformational changes; FRET

1. Introduction

Since the recognition of the integrin family of adhesion receptors in the eighties, the interest in how integrins acquire their receptor capacity for adhesive proteins has driven a great deal of activity [1], which provided new answers and opened up new questions on old aspects, such as their ligand binding affinity and specificity, their mechanism of priming, their diffusion- and/or cytoskeleton-driven mobility, their distribution in the plane of the membrane, the disposition of the different integrin domains with respect to the membrane and the role played by the membrane lipid bilayer. In the last few years, the structural knowledge on integrins improved most significantly, since the crystallographic structures of the recombinant ectodomain of integrin $\alpha_V\beta_3$ and its complex with a RGD peptide were accomplished [2,3]. Although they lack the transmembrane and cytoplasmic domains, these truncated structures revealed a 135° bend, in contrast with the multiple (filled globular, empty oval, head-two-tails and bilobular) conformations of whole integrins in detergent solution observed previously by metal-rotary shadowing and electron microscopy [4–6]. The bent conformation was subsequently confirmed, both by new electron microscopy of the soluble ectodomains of $\alpha_{IIb}\beta_3$ in solution with Ca^{2+} [7] and of the soluble ectodomain of $\alpha_V\beta_3$ and the complex of this ectodomain with a fragment of fibronectin in solution with Mn^{2+} [8], as well as by cross-competition among monoclonal antibodies for $\alpha_{IIb}\beta_3$ in platelets at rest and after activation [9]. These observations, together with the finding that the major change between the liganded and unliganded crystal structures of the soluble ectodomains of $\alpha_V\beta_3$ takes place at the F/α7 loop of the βA domain, led to the proposal of the deadbolt model [10]. In this model, the CD loop of the membrane-proximal βTD domain, which contacts the F/α7 interface of the ligand binding βA domain,

* Corresponding author. Tel.: +34 915619400; fax: +34 915642431.
E-mail address: pilar.lillo@iqfr.csic.es (M.P. Lillo).
[1] On leave from Departamento de Química e Bioquímica, Faculdade de Ciências, Universidade de Lisboa, R. Ernesto de Vasconcelos, P-1749-016 Lisboa, Portugal.

0301-4622/$ - see front matter © 2007 Elsevier B.V. All rights reserved.
doi:10.1016/j.bpc.2007.07.007

locks this domain in its inactive state, being the activation switch for the deadbolt release a still unknown inside–out allosteric coupling mechanism through the integrin transmembrane domains. The extended conformation, however, was predominantly observed in electronmicrographs of soluble ectodomains of $\alpha_{IIb}\beta_3$ in the presence of Mn^{2+}, Ca^{2++} RGD or Mn^{2++} RGD [7], which together with the observation that epitopes that become exposed when integrins are activated are buried in the bent conformation [11], led to the suggestion of the switchblade model for affinity switching, where the bent and extended structures of $\alpha_{IIb}\beta_3$ represent the inactive and the active conformations: the switching would be driven by a still unknown allosteric coupling through the integrin transmembrane domains, involving separation of the α and the β cytoplasmic domains [12], strengthening of the integrin at the knees and exposure or generation of the ligand binding site(s) in the extracellular domain. Today it is assumed that this allosteric coupling in integrins is bidirectional, so that ligand binding outside is followed by changes in the cytoplasmic domains, which lead to outside–in signaling by interaction with the cytoskeleton and/or the intracellular signaling pathways. Different aspects of these working models require further elaboration and experimental tests at the cell level to become established facts. Recently, the fluorescence resonance energy transfer between a fluorescent peptide specifically bound to the $\alpha_4\beta_1$ integrin expressed at the cell surface, as a donor, and a fluorescent lipophilic probe incorporated into the membrane of monoblastoid cells, as an acceptor, was monitored using flow cytometry [13]. The variations in the FRET efficiency between the resting and the Mn^{2+} or chemokine-activated integrin were interpreted as a 5.0 and 2.5 nm changes in the separation distance between the cell surface and the integrin binding pocket, respectively, which led the authors to suggest that these changes are primarily due to the vertical extension of the integrin structure.

Here we will focus on the controversy whether an activated integrin actually stands up in the membrane [14–16]. The average distance between the βA domain of the β_3 subunit and the calf-2 domain of α_{IIb} subunit at rest (about 6 nm) should almost triplicate after platelet activation (about 17 nm), if integrin $\alpha_{IIb}\beta_3$ acquired the extended conformation (Fig. 1), as proposed by the switchblade model. In the present paper, we monitored the FRET efficiency between fluorescently labeled Fab fragments of monoclonal antibodies directed against the α_{IIb} subunit calf-2 domain and the β_3 subunit βA domain of $\alpha_{IIb}\beta_3$, in resting and in activated platelets. We used the same monoclonal antibodies with which we showed before that the conformation of activated $\alpha_{IIb}\beta_3$ is agonist-dependent and that the bent conformation of $\alpha_{IIb}\beta_3$ is present in resting and in activated platelets [9]. The FRET results obtained here are consistent with a conformation less extended than proposed by the switchblade model for activated $\alpha_{IIb}\beta_3$ in living platelets, but they don't exclude possible reorientational changes of the integrin domains in the platelet membrane.

2. Materials and methods

2.1. Fluorescence probes

The amine-reactive probes fluorescein 5-isothiocynate (FITC) and Alexa Fluor 488 carboxylic acid, succinimidyl ester, dilithium salt (A488) were obtained from Molecular Probes, Inc, and carbocyanine Cy3™ monofunctional NHS ester (Cy3) was purchased from Amersham Biosciences. Adenosine-5′-diphosphate (ADP) and the acetoxymethyl ester of fura 2 (fura2-AM) were obtained from Sigma and the peptide TRAP-6 (SFLLRN) from Bachem.

2.2. Isolation and labeling of monoclonal antibodies with fluorescent dyes

Murine B lymphocyte hybridomas secreting monoclonal antibodies (mAb) specific for $\alpha_{IIb}\beta_3$ and its subunits had been obtained according to immunization and fusion protocols and

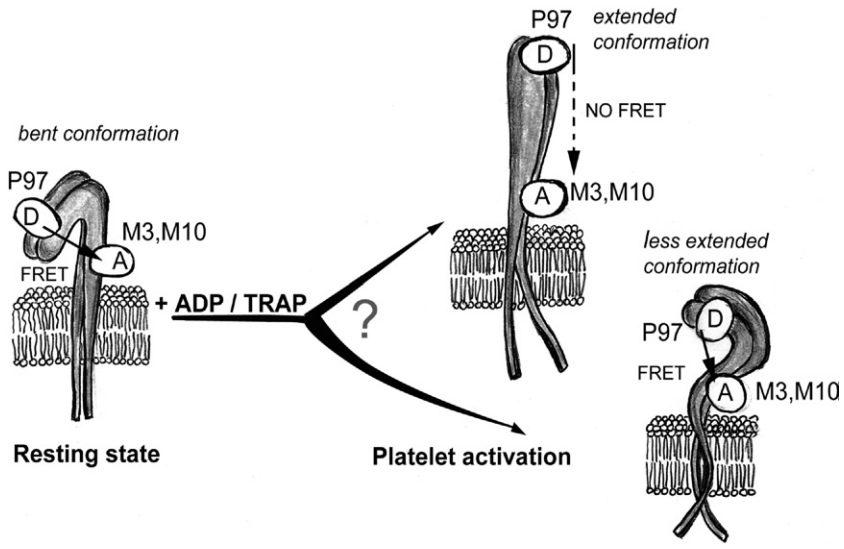

Fig. 1. Cartoon showing the planned FRET experiments. The putative location of the donor (D, anti-β_3) and acceptor (A, anti-α_{IIb}) Fab fragments are represented by D and A labelled ellipses [9].

screening assays described previously [17] and their antibodies, all of the immunoglobulin G (IgG) class, were obtained by growing the specific hybridomas in the peritoneal cavities of mice. We precisely selected the mAbs P97, M3 and M10 for use in the present work, based on their properties: their epitopes are conveniently located at the N-terminal (P97) and the C-terminal (M3 and M10) ends of the ectodomains of the β_3 and α_{IIb} subunits, respectively; their binding to resting and ADP- and TRAP-activated platelets had been well characterized; and P97, by being an aggregation inhibitor, had the further advantage of avoiding any possible platelet aggregation during the spectroscopic measurements after activation ([9] and references therein).

The antibodies were isolated from ascites fluid by 50% saturated $(NH_4)SO_4$ precipitation and affinity chromatography on protein A-Sepharose (Amersham Bioscience), according to the manufacturer's instructions. Fab fragments of these antibodies were prepared by papain digestion at 37 °C, followed by anion exchange chromatography using a Bio-Scale Q2 (Bio-Rad) column and, finally, by size-exclusion chromatography using Superdex 75 (Amersham Bioscience). All the preparation processes were monitored by SDS-PAGE [18], colorimetric protein assay [19] and enzyme immunoassay. The pure Fab fragments were subjected to dialysis overnight at 4 °C against 0.2 M sodium bicarbonate buffer, pH 8.5. Covalent labeling reactions were allowed to proceed in the dark for 1 h at room temperature without stirring at a molar dye to protein ratio between 5 and 10. The labeling reaction was stopped using 1.5 M hydroxylamine, pH 8.5. Labeled Fab fragments were separated from unreacted free probe by extensive overnight dialysis at 4 °C against phosphate-buffered saline, followed by gel filtration through a Sephadex G-50 column equilibrated in the same buffer. The final antibody concentration and the bound label to protein stoichiometry were determined spectrophotometrically, using the following molar absorptivities: $\varepsilon_{495\ nm}=73\,000\ M^{-1}\cdot cm^{-1}$ and $\varepsilon_{280\ nm}=7800\ M^{-1}\cdot cm^{-1}$ for A488 [20], $\varepsilon_{554\ nm}=150\,000\ M^{-1}\cdot cm^{-1}$ and $\varepsilon_{280\ nm}=7500\ M^{-1}\cdot cm^{-1}$ for Cy3 [21], and $\varepsilon_{280\ nm}=67{,}500\ M^{-1}\cdot cm^{-1}$ for the Fab. The labeled Fab fragments were subjected to SDS-PAGE and their biological activity monitored by enzyme immunoassay.

2.3. Isolation of human platelets, platelet counting and in vitro platelet activation measurement

For each experiment, blood samples were collected from 4–5 healthy volunteers, using as anticoagulant 1 volume of 0.129 M trisodium citrate in 9 volumes of blood. Afterwards, a pool of platelet-rich plasma was prepared by sedimentation of red and white blood cells at 100 $\times g$ (r_{av}) for 9 min at room temperature. Finally, washed platelets were prepared by gel filtration on a Sepharose 2B (Amersham Biosciences) column, equilibrated with modified Tyroid's buffer (137 mM NaCl, 2.7 mM KCl, 3.3 mM NaH_2PO_4, 20 mM Hepes, pH 7.4 with 0.2% bovine serum albumin and 5 mM glucose).

Platelet counting and control of platelet shape and appearance were done every day in a Neubauer hemocytometer by phase contrast microscopy. The control of ADP (100 μM) and TRAP (25 μM) activation of unlabeled platelets, both in platelet-rich plasma and in washed platelets in the presence of fibrinogen, was routinely done by the extent of platelet aggregation at 37 °C, using either a spectrophotometer or a microplate reader, being the extent of platelet aggregation above 80–85% and 90–95% for ADP and TRAP, respectively. Given that P97 is an inhibitor of platelet aggregation, ADP and TRAP activation of washed platelet in the absence of fibrinogen was also checked by the change in the intraplatelet Ca^{2+} concentration upon activation of platelets, using Fura 2-AM and a SLM 8000 spectrofluorimeter [22]. The amplitude and time course of the Ca^{2+} concentration changes observed in control platelets were similar to those observed in platelets with unlabeled and fluorescently labeled P97 and M3 or M10 Fab fragments bound to $\alpha_{IIb}\beta_3$ (data not shown). This means that the pairs of Fab fragments used in our FRET measurements do not interfere with platelet activation, in agreement with the different cross-competition patterns among anti-α_{IIb} and anti-β_3 mAbs found before, for resting and activated platelets[9].

2.4. Two-step labeling of integrin $\alpha_{IIb}\beta_3$ in intact platelets with A488-P97 and with Cy3-M3 or Cy3-M10 Fab fragments

To label $\alpha_{IIb}\beta_3$ in resting platelets with the fluorescence donor, platelet-rich plasma was incubated with a saturating concentration of A488-P97 Fab fragment (223 nM, equivalent to 25-fold the dissociation constant (K_d) of P97 mAb) [9] for 1 h at room temperature, in the dark and without stirring. After washing the labeled platelets by filtration through Sepharose 2B, to eliminate the unbound donor, and rising Ca^{2+} and Mg^{2+} up to 1 mM final concentration, the donor-labeled platelets (typically 5×10^4–1×10^5 cells/μL) were labeled with the acceptor by further incubation for 1 h in the dark with a fixed near saturating concentration of the acceptor ($15\times K_d$, Cy3-M3 Fab or Cy3-M10 Fab). Alternatively, in those experiments designed to measure the binding isotherms of Cy3-M3 and Cy3-M10 Fab fragments to A488-P97 Fab-pre-labeled $\alpha_{IIb}\beta_3$ in resting platelets, the washed donor-labeled platelets were incubated with increasing concentrations (0–20 $\times K_d$) [9] of Cy3-M3 (0–280 M) or Cy3-M10 (0–320 nM) Fab fragments, in the same experimental conditions as above. The fluorescence measurements to evaluate the FRET efficiencies were done afterwards. Blanks were prepared equally than the samples to study, either without bound fluorescently labeled Fab fragments or with bound unlabeled Fab fragments.

In experiments with inside–out activated platelets, 50 and 100 μM ADP, or 12.5 and 25 μM thrombin receptor activation peptide (TRAP; final concentrations) were added with brief and gentle mixing (to avoid platelet aggregation), after incubation of the washed donor-labeled platelets with a fixed near saturating concentration of the acceptor ($15\times K_d$, Cy3-M3- or Cy-M10-Fab) for 1 h in the dark. The fluorescence measurements of the samples were carried out at 1 min 20 s and 10 min after platelet activation, *i.e.*, within the early part of the time course of fibrinogen binding to activated platelets [23] and, therefore, within the time period platelet $\alpha_{IIb}\beta_3$ remains activated.

2.5. Steady-state and time-resolved spectroscopic measurements

Absorption spectra were recorded on a Cary 3E UV–Vis or on a Phillips PU8750 spectrophotometer. Fluorescence measurements

were carried out with a SLM 8000 spectrofluorimeter using magic angle conditions (excitation polarizer set vertical and emission polarizer set at 54.7°). The excitation of the donor (A488) was generally at 480 or 493 nm and the emission was monitored at 515 nm, while the excitation and emission wavelengths for the acceptor (Cy3) were 550 and 570 nm, respectively. Typically, spectral bandwidths of 4 and 8 nm were used and the samples in 5×5 mm path-length cuvettes were maintained at room temperature. The blank subtraction was done directly with the spectrometer software, by subtraction of the blank spectra from the corresponding sample spectra.

The steady-state fluorescence anisotropy, $\langle r \rangle$, of the fluorescent probes was measured using Glan–Taylor polarizers as

$$\langle r \rangle = (I_{VV} - G \cdot I_{VH})/(I_{VV} + 2G \cdot I_{VH}) \quad (1)$$

The intensities I_{ij} ($i,j=V,H$) are the steady-state vertical and horizontal components of the fluorescence emission with excitation vertical (I_{VV} and I_{VH}, respectively) and horizontal (I_{HV} and I_{HH}, respectively) to the emission axis. The latter pair of components is used to calculate the G factor ($G=I_{HV}/I_{HH}$) [24]. An adequate blank was subtracted from each intensity reading, before calculating the anisotropy value.

Time-resolved fluorescence intensity measurements were performed by the time-correlated single-photon counting technique using an apparatus previously described [25] and magic angle conditions. The donor (A488) was excited at 491 nm and the emission was monitored at 530 nm (bandwidth 8 nm). A 520 nm cut-on filter was added in the emission side to eliminate the scatter contribution from the platelet suspensions. The timing calibration was 6.11 ps/channel. Measurements were performed on 120 μL samples in 3×3 mm path-length cuvettes. The total fluorescence intensity decays were fitted to a sum of 3 exponential functions by iterative convolution, using nonlinear least squares global methods [26] from the GLOBALS Unlimited (Urbana, IL) general purpose program. The adequacy of the analyses was determined from the reduced weighted sum of squares of residuals and from the visual inspection of the distribution of weighted residuals and the autocorrelation plots. The amplitude average lifetimes $\langle \tau \rangle$ were calculated from the fluorescence intensity decays, according to $\langle \tau \rangle = \sum \alpha_i \tau_i$, where α_i and τ_i are the normalized amplitude and lifetime of each fluorescence decay component i, respectively.

2.6. FRET steady-state and time-resolved distance analysis

The average distances between FRET pairs were calculated by:

$$\langle R \rangle = R_0[(1 - \langle E \rangle)/\langle E \rangle]^{\frac{1}{6}} \quad (2)$$

where $\langle E \rangle$ is the experimental average energy transfer efficiency, R_o is the Förster radius corresponding to 50% energy transfer efficiency, and $\langle R \rangle$ is the average distance between the donor and the acceptor. The average steady-state FRET efficiency was determined from the ratio of the steady-state measurements of the fluorescence intensities for the donor-only (I_D) (λ_{ex}=480 nm, λ_{em}=490–530 nm) and the donor in the presence of the acceptor (I_{DA}) labeled platelets ($\langle E_{SS} \rangle = 1 - I_{DA}/I_D$). The average time-resolved FRET efficiency was determined from the ratio of the average lifetimes for the donor-only ($\langle \tau \rangle_D$) (λ_{ex}=491 nm, λ_{em}= 530 nm) and for the donor in the presence of the acceptor ($\langle \tau \rangle_{DA}$) labeled platelets ($\langle E_{TR} \rangle = 1 - \langle \tau \rangle_{DA}/\langle \tau \rangle_D$). The main purpose of this comparative analysis was simply to determine if the steady-state and the time-resolved FRET efficiencies were internally consistent. Since the time-resolved data do not require knowledge of the absolute concentrations of the donor-only and donor/acceptor samples, uncertainties in the labeled protein concentrations do not contribute to the measured $\langle E_{TR} \rangle$ value. Similarly, the steady-state transfer efficiencies can be affected by static quenching mechanisms, which will not affect the time-resolved signals.

The R_0 in Å for a given donor–acceptor (D–A) pair was determined as:

$$R_0 = 0.2108 \cdot \left[\langle \kappa^2 \rangle \cdot \Phi_D \cdot n^{-4} \cdot J\right]^{\frac{1}{6}} \quad (3)$$

where J (M^{-1} cm^{-1} m^4) is the overlap integral between the normalized donor's emission fluorescence spectra and the acceptor's absorption spectra, Φ_D is the quantum yield of the donor measured using disodium fluorescein in 0.01 M NaOH as a reference (quantum yield=0.95±0.03) [27], n=1.33 is the refractive index of water and $\langle \kappa^2 \rangle = 2/3$ (see above) is the orientation factor.

The binding isotherms of the acceptor-Fab fragment conjugates (ligand) to the integrin $\alpha_{IIb}\beta_3$ in resting platelets were analyzed according to a saturable one-site binding model $\langle E_{ss} \rangle = x_{bound} \cdot \langle E_{lim} \rangle$, where $x_{bound} = [P]_{bound}/[P]_{total}$, the saturation fraction of receptors (P) with ligand (Fab) is a function of total ligand and receptor concentrations, $[Fab]_{total}$ and $[P]_{total}$, respectively, and of the dissociation constant of the ligand, K_d:

$$x_{bound} = \frac{\gamma - \sqrt{\gamma^2 - 4 \cdot [P_{total}] \cdot [Fab_{total}]}}{2 \cdot [P_{total}]}$$
$$\gamma = K_d + [Fab_{total}] + [P_{total}] \quad (4)$$

Since the fluorescence labeling of the donor/acceptor-Fab fragments is not unique for a specific amino group, the interchromophoric distance in the donor/acceptor labelled integrin will not be unique, and a discrete distance will not be able to adequately represent the measured FRET efficiencies. The observed donor decay in the presence of the acceptor will contain multiple contributions with a probability distribution function dependent upon the distribution of donor–acceptor distances ([28] and references therein). Then, in order to better characterize the conformational changes in the integrin, a model of donor–acceptor distance distribution was also used to fit the time-resolved fluorescence data. Hence, the donor–acceptor distance distributions were obtained from direct simultaneous analysis of both the donor-only and donor–acceptor fluorescence decays, by introducing a Gaussian function to describe the shape of the probability of distance distribution, $P(R)$ with

the mean distance, R_m, and the width (standard deviation, σ) as adjustable parameters in the fitting of the donor–acceptor decay data [28].

2.7. Statistical analysis

Data are presented as mean ± SD. Student's *t*-test was used for statistical comparisons between data obtained with resting platelets and with ADP- or TRAP-activated platelets. A p level ≤ 0.05 was considered statistically significant.

3. Results

3.1. Spectroscopic characterization of the fluorescently labeled Fab fragments and their binding to resting and activated platelets

The main goal of this study was to monitor the conformational changes of the integrin $\alpha_{IIb}\beta_3$, which take place after *in vitro* physiological activation of human platelets, using FRET measurements. To place the FRET donor and acceptor probes in the most convenient sites of the integrin, Fab fragments were used instead of the whole IgG by obvious reasons: 1) to decrease the size of the carriers of the fluorescent probes and, in this way, to decrease the uncertainty in the probe location and, therefore, in the calculation of the intramolecular distance we wanted to measure; 2) to avoid the divalency of the probe carrier and the problems this could introduce in the experiment; 3) to avoid binding competition between those antibodies which compete sterically in the IgG form. Thus, the integrin was specifically labeled with suitable donor and acceptor probes by means of the Fab fragments of the monoclonal antibodies P97 (specific for the N-terminal βA domain of the β_3 subunit) and M3 and M10 (specific for the C-terminal calf-2 domain of α_{IIb} subunit) (see Fig. 1 and Table 1). In addition, these mAbs were chosen to perform this study, because their high-affinity binding to whole platelets have been characterized previously, both at rest and upon platelet activation by ADP and TRAP (Table 1) and because the convenience to have P97 to inhibit any platelet aggregation that could take place during these optical experiments [9]. In Table 1 it is also shown the binding sites of A488-P97 Fab per platelet, at rest and after ADP and TRAP activation, determined at a concentration fifteenfold its K_d in the presence of a concentration fifteenfold the K_d of unlabeled M3 and M10 Fabs and, the other way around, the binding sites of Cy3-M3 and Cy3-M10 Fabs per platelet at rest and after ADP and TRAP activation, in the presence of unlabeled P97-Fab.

Table 1
Dissociation constants from whole platelets at rest and after activation by 100 μM ADP or 25 μM TRAP. Binding sites per platelet (mean ± SE) of the IgG forms of the anti-β_3 (P97) and anti-α_{IIb} (M3 and M10) monoclonal antibodies used in the FRET measurements [9] and binding sites of their Fab forms per platelet (*)

mAb (form)	K_d (nM) and [binding sites x 10^{-3}/platelet]		
	Rest	+ADP	+TRAP
P97 (IgG)	9±3 [55±4]	20±3 [39±3]	11±2 [35±1]
P97 (Fab)(*)	[58±4]	[59±4]	[67±5]
P97 (Fab)(*,1)	[56±4]	[53±5]	[63±5]
P97 (Fab)(*,2)	[56±4]	[63 ±3]	[71±2]
M3 (IgG)	16±2 [71±3]	10±2 [60±3]	17±3 [58±4]
M3 (Fab)	[69±4]	[57±4]	[77±6]
M3 (Fab)(*,3)	[68±5]	[65±9]	[69±6]
M10 (IgG)	14±2 [40±2]	21±2 [32±1]	24±3 [34±1]
M10 (Fab)	[34±2]	[48±15]	[37±5]
M10 (Fab)(*,3)	[32±1]	[36±4]	[34±3]

(*) Data from four experiments, determined at a concentration $15 \times K_d$ of A488-P97, Cy3-M3 and Cy3-M10 Fab's, by a bound-phase separation assay in the presence of a concentration $15 \times K_d$ of unlabeled M3-Fab(1), M10-Fab(2) and P97-Fab(3) [9].

Table 2
Summary of the fluorescence properties of the fluorescently labeled Fab fragments in phosphate-buffered saline, pH 7.4

Fab fragment	F/P [a]	$\langle r \rangle_{peak}$ [b]	$\langle r \rangle_{tail}$ [c]	Φ_D [d]
A488-P97	4.2	0.065±0.001	0.082±0.005	0.45±0.01
Cy3-M3	0.9	0.237±0.002		
Cy3-M3	1.6	0.233±0.001	0.241±0.009	
Cy3-M10	1.9	0.195±0.001	0.253±0.012	
FITC-P97	1.1	0.143±0.002		0.63±0.01

[a] Fluorescence label-to-Fab fragment molar ratio.
[b] Steady-state fluorescence anisotropy in solution measured at 493-nm or 550-nm excitation and 515-nm or 565-nm emission for A488- and FITC- or Cy3-labeled monoclonal Fab fragments, respectively.
[c] Steady-state fluorescence anisotropy in solution measured at 515-nm or 570-nm excitation and 530-nm or 590-nm emission for A488- or Cy3-labeled monoclonal Fab fragments, respectively.
[d] Donor fluorescence quantum yield in solution.

The fluorescence emission spectrum of the unbound A488-P97 Fab fragment (donor) overlaps well with the absorption spectrum of unbound Cy3-M3 Fab fragment (acceptor) ($J = 6.22 \times 10^{15}$ $M^{-1}cm^{-1}nm^4$), which together with the determined quantum yield of the donor ($\Phi_D = 0.45$) allowed to calculate a distance of 6.1 ± 0.3 nm for 50% efficiency of FRET (R_0) between this donor–acceptor pair. Given that the excitation and emission spectra and the lifetimes (see below) of donor and acceptor dyes covalently bound to the Fab fragments don't change significantly upon the binding of these fragments to the platelets, the R_0 should be the same for the integrin-bound probes. This high R_0 value is well-suited to measure energy transfer efficiencies between a single donor–acceptor pair over a distance range between 3.0 and 9.0 nm [29] and, therefore, it is expected to be sensitive enough to track large agonist-induced structural rearrangements predicted by the "switchblade" model of integrin activation [16]. The free A488-P97 Fab fragment presented a low steady-state fluorescence anisotropy in solution ($\langle r \rangle_{tail} = 0.082 \pm 0.005$) compared with the higher steady-state fluorescence anisotropy values measured for the Cy3-M3 and Cy3-M10 Fab fragments free in solution ($\langle r \rangle_{tail} = 0.24$–$0.25$, see Table 2), which indicates that the covalently-attached fluorophores displayed different levels of mobility in these proteins, the rotational freedom of the Cy3 probes being the more restricted. The occurrence of significant energy homotransfer between the multiple labeled Fab fragments can also be inferred from the 26% and 30% relative increase in the fluorescence anisotropy of A488-P97 and Cy3-M10, respectively,

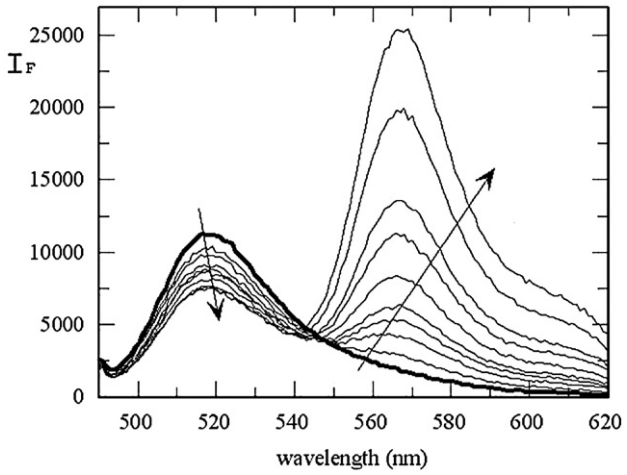

Fig. 2. FRET measurements between fluorescently labeled Fab fragments (A488-P97 and Cy3-M10) bound to integrin $\alpha_{IIb}\beta_3$ in resting platelets. Fluorescence emission spectra (λ_{ex}=480 nm) of platelets pre-labeled with a saturating concentration of donor A488-P97 Fab (223 nM), after eliminating the unbound donor by gel filtration and subsequent incubation (for 1 h, in the dark and at room temperature) with increasing concentrations of the acceptor C3-M10 Fab (from 0 to 280 nM). The downwards and upwards arrows show the saturable quenching of the donor fluorescence and the contribution of the linear increase of fluorescence of the acceptor excess, respectively, as a function of the increasing acceptor concentration.

when the excitation wavelength was moved from the peak to the tail of their absorption spectrum (Table 2). Both the multiple labeling and segmental mobility of the bound dyes warrants the use of $<\kappa^2>=2/3$, *i.e.* the isotropic dynamic limit for the orientation factor, used in the calculation of R_0.

3.2. FRET efficiency measurements between $\alpha_{IIb}\beta_3$-bound donor/acceptor pairs in resting platelets: binding isotherms of Cy3-M3 and Cy3-M10 Fab fragments to A488-P97 Fab-pre-labeled $\alpha_{IIb}\beta_3$ in resting platelets

Fig. 2 illustrates a typical experiment showing that the interaction of Cy3-M10 Fab fragment with integrin $\alpha_{IIb}\beta_3$ could be monitored by the quenching of the fluorescence from the A488-P97 Fab fragment pre-bound to the fibrinogen receptor in resting platelets. After removing free A488-P97 Fab fragments from the samples by gel filtration, the donor-labeled platelets were incubated with increasing concentrations of the acceptor and the emission spectra exciting at 480 nm were measured (Fig. 2). It is observed an increasing quenching of the donor-Fab bound when the acceptor-Fab concentration is increased. The extension of this quenching is consistent with the dynamic quenching of the donor fluorescence lifetime in the presence of the acceptor determined for the same samples (see below), which indicates that FRET is apparent for the donor–acceptor pairs described in this study. The fluorescence intensity at 570 nm (acceptor side) does not follow the FRET pattern. It is near a linear function of the total acceptor concentration in solution, due to direct acceptor excitation. Fig. 3 represents the binding isotherms of the Cy3-M10 and Cy3-M3 Fab fragments to resting platelets pre-labeled with A488-P97 Fab, in terms of steady-state average FRET efficiencies,$<E_{SS}>$. These values are essentially "model-independent", in that they are simply experimental determinations of the ratio of fluorescence for the donor-only and donor–acceptor labeled species in the donor side of the emission spectra (490–530 nm range). Due to the inverse sixth power dependence of the resonance energy transfer rate constant with the separating distance between a donor–acceptor pair [29], only the fluorescently-labeled P97 and M10 Fab or M3 fragments brought into close proximity upon binding to different epitopes located on the same integrin $\alpha_{IIb}\beta_3$ could originate intersubunit FRET (see Discussion) and, therefore, the data in Fig. 3 would correspond to the binding isotherms of the Cy3-M10 and Cy3-M3 Fab fragments to the fibrinogen receptor pre-labeled with the A488-P97 Fab fragment. A single class of saturable binding sites model would fit the FRET data, yielding limiting FRET efficiencies of 0.318±0.007 and 0.23±0.01 for the two platelet bound donor–acceptor pairs studied here, A488-P97/Cy3-M10 and A488-P97/Cy3-M3 respectively (Fig. 3), and binding constants (K_d) of the same magnitude than those determined before (Table 1 and [9]).

When the donor-labeled platelets were titrated with unlabeled M3 and M10 Fab fragments, no significant decrease of A488 fluorescence intensity (λ_{ex}=480 nm, λ_{em}=490–530 nm) occurred, precluding the occurrence of direct or indirect local fluorescence quenching of the A488 dye by the unlabeled M3 or M10 Fab fragments (*e.g.*, due to conformational changes induced by the binding of the second Fab fragment to the integrin $\alpha_{IIb}\beta_3$). As an additional control to establish the stability of the receptor-bound P97-A488 Fab fragment, its steady-state fluorescence anisotropy was monitored for 4 h, the approximate time necessary to perform the FRET steady-state

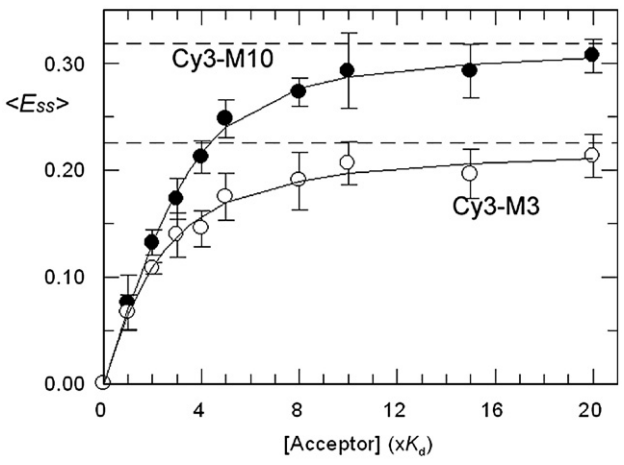

Fig. 3. Binding isotherms of the Cy3-M10 (●) and Cy3-M3 (○) Fab fragments to resting platelets pre-labeled with the A488-P97 Fab measured by steady-state FRET. The energy transfer efficiency, <*Ess*>, is represented as a function of the acceptor concentration, expressed as multiples of the respective whole mAb dissociation constants for binding to resting platelets: K_d(M10)=14 nM and K_d (M3)=16 nM (Calzada et al. 2002). The limiting energy transfer efficiencies, $<E>_{lim}$, between platelet-bound donor–acceptor pairs were obtained from fitting the saturable one-site binding model (Eq. (4)) to the experimental data, by a nonlinear least squares regression (solid curves): $<E_{lim}>=0.318\pm0.007$ (n=3) and $<E_{lim}>=0.23\pm0.01$ (n=3) for A488-P97/Cy3-M10 and A488-P97/Cy3-M3, respectively (n is the number of experiments).

and time-resolved experiments described above. The steady-state anisotropy of A488-P97 Fab,<r> (ex 493 nm, em 515 nm), increases from 0.065±0.001 to 0.15±0.01 when it is bound to $\alpha_{IIb}\beta_3$. The bound anisotropy value (0.15) corresponds to the infinite dilution limit. It is important to note that platelet suspensions are strongly scattering samples and the measured anisotropy changes with sample turbidity [30]. No significant decrement of the bound A488-P97 anisotropy was observed, confirming that the off-rate of P97-A488 Fab fragments from the resting receptor state was very slow, in accordance with the high-affinity binding constant measured before for the P97 mAb bound to whole platelets (Table 1).

The fluorescence intensity decays of free (in modified Tyroid's buffer) and platelet-bound A488-P97 Fab fragments were also measured. The best fit to both curves was obtained with a three-exponential decay, as evaluated from a random distribution of the residuals and auto-correlation plots (not shown). The amplitude average lifetime of the donor slightly increased from 2.0 to 2.2 ns upon A488-P97 binding to integrin $\alpha_{IIb}\beta_3$. Time-resolved fluorescence quenching measurements of platelet-bound A488-P97 Fab fragment in the presence of a near saturation concentration of acceptor (15-fold × the K_d's of M3 and M10 mAbs from resting platelets; Table 1) were also carried out. A typical time-resolved FRET experiment corresponding to A488-P97 Fab/Cy3-M3 Fab labeled platelets is presented in Fig. 4. For the two FRET pairs studied, it was observed a dynamic quenching of the fluorescence lifetime of the donor in the presence of the acceptor. The calculated average time-resolved energy transfer efficiencies (Table 3) showed good agreement with their corresponding steady-state measurements (<E_{TR}>=0.29±0.03 and <E_{TR}>=0.21±0.01 for the two donor–acceptor pairs studied, A488-P97/Cy3-M10 and A488-P97/Cy3-M3, respectively), ruling out the contribution of static quenching or inner filter effects to this FRET assay.

The availability in the lab of a P97 Fab fragment fluorescently labeled with FITC, and at a much lower dye-to-protein ratio of 1.1, allowed us to repeat the binding isotherm of Cy3-M3 Fab fragments (dye/protein ratio of 0.9, Table 2) to resting platelets pre-labeled with FITC-P97 Fab fragments. Again, the data were well fitted to a saturable one-site binding model and a slightly larger limiting energy transfer efficiency<E_{lim}>=0.25±0.04 was determined this time (data not shown). This result agrees well with the fact that although the epitopes explored in the integrin $\alpha_{IIb}\beta_3$ structure were not changed in this experiment, the R_0 calculated for the new FITC/Cy3 pair was approximately 5% larger than the R_0 for A488/Cy3 ($J_{FITC/Cy3}=5.83\times10^{15}$ $M^{-1}cm^{-1}nm^4$; $R_0=6.4\pm$ 0.3 nm). This experiment also shows that multiple labeling of P97 or M3 Fab fragments with donors and acceptors, respectively, did not have a strong influence on the final result, suggesting that the determination of average donor–acceptor distances for comparative purposes is valid in our case.

3.3. Calculation of the distance between the donor/acceptor pairs A488-P97/Cy3-M3 and A488-P97/Cy3-M10 bound to $\alpha_{IIb}\beta_3$ in resting platelets

An average separation between each donor–acceptor FRET pair studied was calculated from the limiting energy transfer efficiencies measured, <E_{lim}>, assuming the existence of a single D–A FRET pair separated by a fixed distance (see Discussion). In this way, an <R> of 7.0±0.3 nm was obtained for the bound A488-P97/Cy3-M10 pair and <R> values of 7.5±0.3 and 7.7± 0.3 nm were calculated for the A488-P97/Cy3-M3 and FITC-P97/Cy3-M3 pairs, respectively, bound to resting platelets.

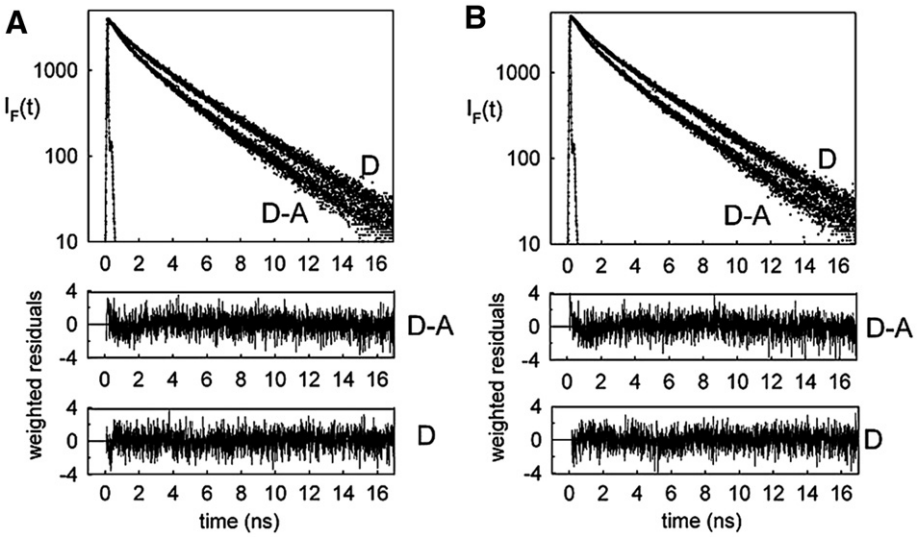

Fig. 4. Time-resolved FRET measurements of resting (A) and ADP activated (B) platelets fluorescently labeled with donor A488-P97 (D) and donor–acceptor A488-P97- Cy3-M3 (D–A) Fab fragments bound to $\alpha_{IIb}\beta_3$integrin. (A) Fluorescence total intensity decays of gel-filtered platelets labeled with donor A488-P97 Fab (D) and gel-filtered platelets prelabeled with donor A488-P97 Fab and incubated with 210 nM acceptor Cy3-M3 Fab (D–A). (B) inside–out platelet activation was done by addition of 100 μM ADP to the labeled donor–acceptor platelets. λ_{ex}=491 nm, λ_{em}=530 nm+520 nm cut-on filter, 8 nm bandwidth, 6.11 ps/channel. T=23 °C. The global fit of the D and D–A decays (see Methods) to the parameters of distance distribution, listed in Table 3, is shown as solid lines. The randomly distributed weighted residuals are shown below.

Table 3
Effect of the inside–out activation of platelets by ADP or TRAP on the FRET energy transfer efficiencies and distance distributions between the platelet-bound anti-β_3 A488-P97 Fab fragment (donor) and anti-α_{IIb} Cy3-M10 or Cy3-M3 Fab fragments (acceptors)

D–A pair	Sample	$<E_{ss}>$ [a]	$<E_{TR}>$ [b]	$<R_{ss}>$ (nm) ±0.4	R_m [c] (nm) ±0.4	σ [d] (nm) ±0.2
A488-P97/ Cy3-M10	Resting platelets	0.27±0.03	0.29±0.03	7.2	8.2	1.1
	+ADP 50 μM	0.24±0.01		7.4		
	+ADP 100 μM	0.24 [e]±0.01	0.24±0.01	7.4	8.5	1.3
	+TRAP 12.5 μM	0.22 [e]±0.02		7.5		
	+TRAP 25 μM	0.23 [e]±0.01	0.27±0.01	7.5	8.3	1.3
A488-p97/ Cy3-M3	Resting platelets	0.19±0.03	0.21 ±0.01	7.8	8.3	1.0
	+ADP 50 μM	0.24 [e]±0.03		7.4		
	+ADP 100 μM	0.23 [e]±0.02	0.22±0.01	7.5	8.1	0.9
	+TRAP 12.5 μM	0.23 [e]±0.02		7.5		
	+TRAP 25 μM	0.23 [e]±0.02	0.23±0.01	7.5	8.0	0.9

[a] Steady-state average energy transfer efficiency.
[b] Time-resolved average energy transfer efficiency. $<E_{TR}>$ and $<E_{SS}>$ data are the means±standard deviations from duplicate and at least triplicate determinations of time-resolved and steady-state measurements, respectively.
[c] Mean value of the Gaussian donor–acceptor distance distribution.
[d] Standard deviation of the Gaussian donor–acceptor distance distribution. See the legend of Fig. 4 for experimental details.
[e] $p \leq 0.05$ for the differences between unstimulated and ADP- or TRAP-stimulated platelets determined by Student's t test for paired samples.

The analysis of the time-resolved FRET data to a discrete distance model was not satisfactory for any of the studied distances. Global analysis of the donor-only and donor–acceptor decays, in terms of a single distributed donor–acceptor distance yielded the best χ^2 and random residual patterns with the least number of adjustable fitting parameters. Random labeling of the Fab fragments, Fab conformational flexibility, orientational factor, and the length and flexibility of the linker of the donor and acceptor probes may be contributing to this distribution. The mean distance values obtained from these analyses were $R_m = 8.2 \pm 0.4$ nm ($\sigma = 1.1 \pm 0.2$ nm) and $R_m = 8.3 \pm 0.4$ nm ($\sigma = 1.0 \pm 0.2$ nm) for A488-P97/Cy3-M10 and the A488-P97/Cy3-M3 pairs bound to resting platelets, respectively (Table 3 and Fig. 5). Although this approach gives 10–15% higher mean distance values, the relative distance changes are of the same order than those found using the average lifetime values. In Table 3 we present the average steady-state and time-resolved energy transfer efficiencies and the distance distribution parameters recovered from the time-resolved analysis.

3.4. Influence of inside–out platelet activation on FRET measurements between $\alpha_{IIb}\beta_3$-bound donor–acceptor pairs

The final series of experiments addressed whether physiological agonists (ADP and thrombin), acting through different inside–out signaling pathways [31], caused activation-related conformational changes of the fibrinogen receptor, the integrin $\alpha_{IIb}\beta_3$, consistent with any of the two forms of the integrin and with any of the two integrin activation models that have been proposed before [15]. ADP interacts with P2 receptors on the cell surface, initiating several signal transduction cascades [32]. The mechanism of platelet activation by thrombin involves the protolytic cleavage of the 41 amino acid residue N-terminal fragment of the G-coupled Protease-Activated Receptor 1. The new N-terminal sequence SFLLRN of the cleaved receptor acts as an intramolecular ligand and starts the transmembrane signaling process [33]. The synthetic peptide TRAP-6 interacts with this receptor [34] and allows to induce platelet activation without the use of thrombin.

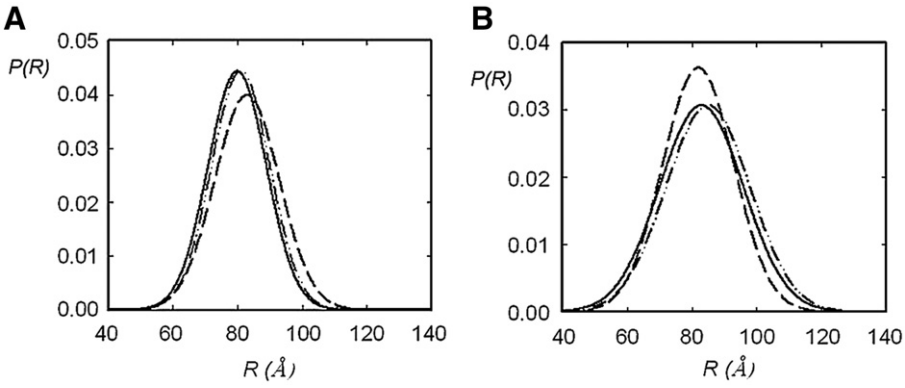

Fig. 5. Effect of inside–out activation of platelets by ADP and TRAP, on the Gaussian distance distributions between the platelet-bound anti-β_3 A488-P97 Fab fragment (donor) and the anti-α_{IIb} Cy3-M3 (A) and Cy3-M10 (B) Fab fragments (acceptors). Gel-filtered platelets pre-labeled with a saturating concentration of the donor A488-P97 Fab were incubated either with 210 nM Cy3-M10 Fab or 240 nM Cy3-M3 Fab (corresponding to 15× the K_d of the respective whole mAb). Inside–out platelet activation was done by addition of 100 μM ADP or 25 μM TRAP (final concentration) to the platelet suspension with brief and gentle mixing. The probability of energy transfer distance distributions, $P(R)$, recovered from the global analysis of the time-resolved fluorescence decays of donor and donor/acceptor Fab labeled samples are plotted for resting platelets (— — —), ADP- (—·—·—) and TRAP- (——) activated platelets.

Table 3 summarizes the steady-state and time-resolved FRET efficiency results obtained after the addition of ADP and TRAP to platelets dually labeled with the donor–acceptor FRET pairs used in resting platelets. The experiments were carried out using a fixed near saturating concentration of acceptor-labeled Fab fragment, as described above, which yielded near maximal fluorescence quenching and corresponded to 15-fold its dissociation constant from resting platelets. Platelet activation by 100 μM ADP or 25 μM TRAP produced about an 11% and 15% decrease, respectively, in the mean steady-state FRET efficiencies measured between platelet-bound A488-P97 and Cy3-M10 Fab fragments. These changes were statistically significant ($p<0.02$ and $p<0.01$, respectively) and represent about ~0.2–0.3 nm increase in the calculated average separation distance. In contrast, the same agonists produced a small increase of about 21% ($p<0.04$) in the FRET efficiency between the other donor–acceptor pair studied, A488-P97/Cy3-M3, in 100 μM ADP or 25 μM TRAP-activated platelets, which represent about ~0.2–0.3 nm decrease in the calculated average separation distance. The activation-induced changes of FRET efficiency were not time-dependent within the ~10-min observation period of our measurements. The time-resolved FRET measurements performed with the same samples confirmed that neither of the physiological agonists used was able to produce dramatic distance changes in $\alpha_{IIb}\beta_3$ (Figs. 4 and 5 and Table 3).

In control experiments with platelets labeled with A488-P97 alone, we found that neither the fluorescence intensity decay kinetics of the donor, nor its steady-state fluorescence anisotropy, were affected by platelet activation with ADP or TRAP (not shown), which demonstrates that the fluorescence properties of A488 and the binding constant of donor-labeled Fab fragments to the activated fibrinogen receptor were not influenced by platelet stimulation induced by any of these agonists.

4. Discussion

4.1. Considerations on the possible limitations to the reliable distance determinations by the FRET methodology

(1) *Contribution of inter-integrin FRET* — There are approximately $5–8\times10^4$ copies of integrin $\alpha_{IIb}\beta_3$ per platelet. We also know that $\alpha_{IIb}\beta_3$ represents 21% of the intrinsic proteins of the platelet plasma membrane [35], where it is randomly distributed both in resting and in activated platelets in the absence of fibrinogen [36–38]. Thus, because our objective requires to measure only intersubunit FRET within individual integrins, it is necessary to evaluate the potential contribution of intersubunit FRET between neighboring $\alpha_{IIb}\beta_3$ integrins to the measured FRET efficiencies for each donor–acceptor pair studied. From the number of phospholipids (ph) and cholesterol (ch) molecules per $\alpha_{IIb}\beta_3$ molecule in the membrane [35] and from the cross-section areas of these molecular species, we can estimate that the average surface area occupied by an integrin plus its surrounding cholesterol and phospholipid molecules is of about 666 nm^2 (800 ± 50 ch molecules/$\alpha_{IIb}\beta_3$) × 0.4 nm^2/ch]/2 = 160 nm^2 of ch occupied area; 1200 ± 40 ph molecules/$\alpha_{IIb}\beta_3$) × 0.71 nm^2/ph)]/2 = 426 nm^2 of ph occupied area; 80 nm^2 occupied by an integrin molecule with a 5 nm radius). This corresponds to an integrin density of 0.054 (36 nm^2/666 nm^2), as calculated in units of number of integrin molecules/R_0^2 (R_0 = 6 nm). Using the simple series approximation derived by Wolber and Hudson [39], that describes the energy transfer between a random distribution of donors and acceptors on an infinite plane, and considering an exclusion radius around each donor equal to the integrin radius, an energy transfer efficiency of 0.06 is predicted for the inter-integrin FRET contribution between the integrin-bound A488-P97/ Cy3-M10 and A488-P97/ Cy3-M3 donor–acceptor pairs. It should be noted that this is an overestimation of the real value due to several approximations used above: (a) the calculation of the surface concentration of integrin in the platelet membrane did not include the area occupied by the other intrinsic proteins; (b) the donors and acceptors were considered to be on the same plane, and (c) the distance of closest approach, or exclusion radius around each integrin was approximate to the protein radius. Therefore, it can be safely concluded that the inter-heterodimer FRET contribution to our FRET efficiency measurements is almost negligible in our experimental conditions.

(2) *Heterogeneity in the labeling of the Fab fragments used with donor and acceptor fluorophores* — A decisive argument against the relevance of the multiple fluorescent labeling of the Fab fragments (Table 2) on the distance calculations carried out in this study is that when we substituted the donor/acceptor pair A488-P97/ Cy3-M3 (with a dye to protein molar ratio of 4.2 and 1.6, respectively) for FITC-P97/ Cy3-M3 (with a dye to protein molar ratio of 1.1 and 0.9, respectively) the final results did not change significantly. Furthermore, the 1 nm width of the distance distributions, recovered in all the cases from the analysis of the time-resolved FRET measurements, gives us a good estimation of the contribution of the uncertainty in the location of the binding sites of the fluorophores within each Fab, the length and flexibility of the donor and acceptor probes, and the Fab dynamics to the recovered distance determinations.

(3) *Size of the Fab fragments* — A potential drawback to the use of randomly fluorescently-labeled Fab fragments is that their effective size is comparable to the molecular distances being measured. However, it should be stressed that for experiments designed to detect conformational changes, as in the present study, precise placement of the donor and acceptor probes is not essential, since changes in average distances are of primary interest rather than absolute site to site distance measurements. The switchblade model predicts that integrin $\alpha_{IIb}\beta_3$ adopts an extended conformation upon platelet activation and, accordingly, the average separation distance between the βA domain of the β_3 subunit and the calf-2 domain of the α_{IIb} subunit is expected to increase almost 3-fold (ΔR ~ 100 nm) with activation. In this

situation, the energy transfer between the donor and the acceptor after platelet activation should be completely abolished (Fig. 1), as the distance would be too large to be measured by FRET, using a donor–acceptor pair with a R_0~6 nm. However, the measured FRET efficiencies after activation were almost unchanged.

(4) *Degree of Platelet and Integrin Activation and Donor and Acceptor Fab Binding Sites per Platelet and their influence on FRET measurements and intramolecular distance calculations* — Several facts allow us to estimate that a large majority of integrin $a_{IIb}\beta_3$, in the labeled and activated platelet suspensions used for FRET, are activated and nearly saturated with donor and acceptor Fabs. On the one hand, the use of high agonist concentrations (0.1 mM ADP and 25 mM Trap) allows getting over 80–85% and 90–95% platelet activation for ADP and TRAP, respectively, which means over 90% integrin activation. On the other hand, at the concentration used for binding of donor A-488 P97 Fab and acceptors Cy3-M3 Fab and Cy3-M10 Fab to platelets, over 94% of the integrins should be saturated with both donor and acceptor. In addition, the donor remains bound for at least four hours, as deduced from the constant steady-state anisotropy of A-488-P97 Fab bound to pre-labeled filtered platelets and the acceptors remain equally bound, because the concentration of free acceptor was maintained there during all the FRET measurement stage and because the FRET observed between donor A488-P97 Fab and acceptors C3-M3 Fab and Cy3-M10 Fab increases as the concentration increases up to a saturation level (the limiting FRET efficiency) in both resting and activated platelets, as observed by steady-state and by time-resolved measurements.

4.2. Low-affinity conformation of Integrin $\alpha_{IIb}\beta_3$, probed by intramolecular FRET at the surface of resting platelets

Our hypothesis in this study was that if platelet activation by physiological agonists, ADP and TRAP, induced large changes in the bent conformation of integrin $\alpha_{IIb}\beta_3$, they should be directly detectable with an optimized FRET assay. FRET is a well-established method for measuring distances in the 1.0 to 10 nm range and it is often used for monitoring conformational changes of proteins, both in solution and when bound to membranes. The FRET protocol developed here was optimized with respect to previously published procedures [40,41] by: (a) the use of fluorescently-labeled Fab fragments instead of mAbs, to decrease their size and valency and avoid their competition; (b) the selection of a donor–acceptor pair with a higher R_0 value, to increase the precision of the FRET measurements; (c) the performance of both steady-state and time-resolved fluorescence measurements, to rule out possible experimental artifacts in the assay; and (d) the characterization with high precision of the binding isotherms of the acceptor-conjugated Fab fragments to unstimulated platelets pre-labeled with donor-conjugated Fab fragments, to define a basal FRET efficiency (Fig. 3) and to validate the optimized FRET assay. From the limiting energy transfer efficiencies, obtained by fitting a simple saturable one-site binding model to the steady-state experimental data, we calculated an average separation in the range of 7.0–7.5 nm for the two donor–acceptor pairs studied, when they are bound to the resting low-affinity bent conformer of integrin $\alpha_{IIb}\beta_3$. If we consider that the average diameters of an epitope and of a Fab fragment are 3 nm and 6 nm, respectively, the 7.0–7.5 nm average separation found is slightly larger than the average distance between the centers of mass of two Fab fragments bound side by side to the same antigen, as one would expect for the P97/M3 and P97/M10 Fab pairs, whose fragments bind close to each other to the resting and bent conformation of $\alpha_{IIb}\beta_3$, but without overlapping [9]. Thus, our results confirm that the N-terminal domain of the β_3 subunit is very close to the extracellular C-terminal end of the α_{IIb} subunit and, once more, confirm the bent conformation of the integrin in resting platelets.

4.3. Integrin $\alpha_{IIb}\beta_3$ high-affinity conformation probed by intramolecular FRET in activated platelets

ADP- and TRAP-triggered platelet activation had small, although opposite effects, on the two donor–acceptor pairs studied. The FRET efficiency results (Table 3) show, on the one hand, that stimulation of platelets either with ADP or TRAP caused a slight increase in FRET efficiency between fluorescently-labeled P97 and M3 Fab fragments, which reflects a slight increase in their proximity, compared to resting platelets, as one would expect for two antibodies which in their IgG form compete with each other for binding to $\alpha_{IIb}\beta_3$ in ADP-, although not in TRAP-, activated platelets [9]. On the other hand, platelet activation mediated by this physiological agonist is associated with a small decrease of FRET efficiency for the A488-P97/Cy3-M10 pair, which reflects a slight decrease in their proximity in activated $\alpha_{IIb}\beta_3$, compared with resting platelets. Changes in the orientation factor of the donor–acceptor FRET pair *per se* are highly unlikely to justify these results, due to both, the low steady-state fluorescence anisotropy measured for the platelet-bound A488-P97 Fab fragment and the energy migration between the multiple fluorophores covalently attached to each Fab fragment. These results are consistent with previous cross-competition studies among these anti-β_3 and anti-α_{IIb} mAbs carried out before in resting and activated platelets [9]. We should stress that in neither case of inside–out platelet activation was FRET drastically reduced or abolished, as it would have happened if the βA domain of the β_3 subunit at the headpiece, where the P97 mAb epitope is located, had moved more than 3 to 10 nm outward the calf-2 domain of α_{IIb} subunit at the tailpiece, where the M3 and M10 epitopes are located close to the membrane surface, that is, if the integrin conformation had shifted from the bent to the extended form after activation, as predicted by the switchblade model of integrin activation (Fig. 1).

Our findings are consistent with other observations such as the capacity of the bent conformation of the $\alpha_V\beta_3$ full-length ectodomain to stably bind RGD peptides and a fragment of fibronectin (domains 7 to 10 and EDB), as found by X-ray crystallography [3] and electron microscopy [8], respectively. Thus, these and our observations are neither consistent with the

fully extended structure of the soluble full-length $\alpha_V\beta_3$ ectodomain in the presence of Mn^{2+} or Mn^{2++} a cyclic RGD peptide, as observed by electron microscopy [7] nor with the interpretation of energy transfer experiments on Mn^{2+} and chemokine-activated $\alpha_4\beta_1$ integrin in U937 monoblastoid cells and in U937 cells transfected with the formil peptide receptor [13,42]. The discrepancies with Takagi et al. [7] may come from the significant modifications introduced in the recombinant full-length ectodomain they used and from the image selection and data processing methods they employed, as already pointed out by Adair et al. [8]. However our observations may be consistent with Chigaev et al. [13] results. They used a peptide donor specifically bound to the $\alpha_4\beta_1$-integrin and octadecyl rhodamine acceptors incorporated into the plasma membrane, and assumed that the integrin-bound donors and acceptors were randomly distributed in the cell membrane, both in resting and activated platelets. They determine a 2.5 and 5.0 nm distance increase between the peptide donor, at the ligand binding site of the integrin, and the acceptors partitioned into the cell plasma membrane, but one would expect changes of 10 nm or more for a full-extension of the integrin structure after its chemokine or Mn^{2+} activation, respectively. The proposed "less extended" conformation of the active integrin (Fig. 1) may include changes in the perpendicular orientation of the bottom part of the integrin stalk to a more angled orientation or even to a parallel orientation with respect to the plane of the membrane, with the consequent separation of the integrin head from the membrane surface.

5. Conclusions

The molecular mechanisms that couple inside–out agonist-induced platelet stimulation to integrin $\alpha_{IIb}\beta_3$ activation are not well understood yet. In this study, we have shown that platelet activation by the physiological agonists ADP and TRAP is not associated with long-range changes in the separation of the epitopes within integrin $\alpha_{IIb}\beta_3$ probed with chosen Fab fragments labeled with the donor–acceptor pairs A488/Cy3. This result is in agreement with the data previously obtained from cross-competition studies carried out among anti-β_3 and anti-α_{IIb} mAbs directed to the head and leg segments of this heterodimeric protein, both at rest and after platelet treatment with the same activating agents [9], as well as with the bent conformation observed previously in a complex of the ectodomain of $\alpha_V\beta_3$ with a RGD peptide by X-ray crystallography [3] and, most recently, in a complex of this ectodomain with a fragment of fibronectin (domains 7 to 10 and EDB) by electron microscopy [8]. Our observations suggest that integrin $\alpha_{IIb}\beta_3$ does not have to undergo large scale rearrangements in the living cell, to accomplish its physiological role upon inside–out agonist-activation of platelets.

Acknowledgements

We thank A.U. Acuña for stimulating discussions, R. Fernández and G. Bernabeu for their excellent technical assistance, and the technical personnel of the Hematology Service of the Hospital La Paz (Madrid) for collecting the blood samples from normal volunteers. A.Coutinho acknowledges the research grant SFRH/BPD/11667/2002 from F.C.T., Portugal. This work was supported by grants SAF/2003-04266 and BFU2006-03905 (CICYT).

References

[1] R.O. Hynes, Integrins: bidirectional, allosteric signaling machines, Cell 110 (2002) 673–687.
[2] J.P. Xiong, T. Stehle, B. Diefenbach, R. Zhang, R. Dunker, D.L. Seott, A. Joaehimiak, S.L. Goodman, M.A. Arnaout, Crystal structure of the extracellular segment of integrin alpha V beta 3, Science 294 (2001) 339–345.
[3] J.P. Xiong, T. Stehle, R. Zhang, A. Joaehimiak, M. Fraeh, S.L. Goodman, M.A. Arnaout, Crystal structure of the extracellular segment of integrin alpha V beta 3 in complex wit an Arg–Gly–Asp ligand, Science 296 (2002) 151–155.
[4] N.A. Carrel, L.A. Fitzgerad, B. Steiner, H.P. Erickson, D.R. Philips, Structure of human platelet membrane glycoproteins IIb and IIIa as determined by electron microscopy, J. Biol. Chem. 260 (1985) 1743–1749.
[5] M.V. Nermut, N.M. Gree, P. Eason, S.S. Yamada, K.M. Yamada, Electron microscopy and structural model of human fibronectin receptor, EMBO J. 7 (1988) 4093–4099.
[6] G.A. Rivas, J.A. Aznarez, P. Usobiaga, J.L. Saiz, J. González-Rodríguez, Molecular characterization of human platelet integrin GPIIb/IIIa and its constituent glycoproteins, Eur. Biophys. J. 19 (1991) 335–345.
[7] J. Takagi, B.M. Petre, T. Walz, T.A. Springer, Global conformational rearrangements in integrin extracellular domains in outside–in and inside–out signaling, Cell 110 (2002) 599–611.
[8] B.D. Adair, J.P. Xiong, C. Maddock, S.L. Goodman, M.A. Arnaout, M. Yeager, Three-dimensional EM structure of the ectodomain of integrin $\alpha_V\beta_3$ in a complex with fibronectin, J. Cell Biol. 168 (2005) 1109–1118.
[9] M.J. Calzada, M.V. Alvarez, J. González-Rodríguez, Agonist-specific structural rearrangements of integrin $\alpha_{IIb}\beta_3$. Confirmation of the bent conformation in platelets at rest and after activation, J. Biol.Chem. 277 (2002) 39899–39908.
[10] J.P. Xiong, T. Stehle, S.L. Goodman, M.A. Arnaout, New insights into the structural basis of integrin activation, Blood 102 (2003) 1155–1159.
[11] N. Beglova, S.C. Blacklow, J. Takagi, T.A. Springer, Cystein-rich module structure reveals a fulcrum for integrin rearrangement upon activation, Nat. Struct. Biol. 9 (2002) 282–287.
[12] O. Vinogradova, A. Velyvis, A. Velyviene, B. Hu, T.A. Hass, E.F. Plow, J. Qin, A structural mechanism of integrin $\alpha_{IIb}\beta_3$ inside–out activation as regulated by its cytoplasmic face, Cell 110 (2002) 587–597.
[13] A. Chigaev, T. Buranda, D. Dwyer, E.R. Prossnitz, L.A. Sklar, FRET detection of cellular α4-integrin conformational activation, Biophys. J. 85 (2003) 3951–3962.
[14] M.J. Humphries, P.A. McEwan, S.J. Barton, P.A. Buckley, J. Bella, A.P. Mould, Integrin structutre: heady advances in ligand binding, but activation still makes the knees wobble, Trend Biochem. Sci. 28 (2003) 313–320.
[15] M.A. Arnaout, B. Mahalingam, J.P. Xiong, Integrin structure, allostery, and bidirectional signalling, Annu. Rev. Cell Dev. Biol. 21 (2005) 381–410.
[16] B.H. Luo, T.A. Springer, Integrin structures and conformational signalling, Curr. Opin. Cell Biol. 18 (2006) 579–586.
[17] J.A. Melero, J. González-Rodríguez, Preparation of monoclonal antibodies against glycoprotein IIIa of human platelets. Their effects on platelets aggregation, Eur. J. Biochem. 141 (1984) 421–427.
[18] U.K. Laemmli, Cleavage of structural proteins during the assembly of the head of bacterio-phage T4, Nature 277 (1970) 680–685.
[19] C.H. Harrington, Lowry protein assay containing sodium dodecyl sulfate in microtiter plates for protein determinations on fractions from brain tissue, Anal. Biochem. 87 (1990) 206–210.
[20] R.P. Haugland, The Handbook, A guide of Fluorescent Probes and Labeling Technologies, 10th ed, Molecular Probes. Invitrogen Detection Technologies, 2005.

[21] P.I. Bastiaens, T.M. Jovin, in: J. Celis (Ed.), Fluorescence resonance energy transfer microscopy, Cell Biology: A Laboratory Handbook, 2nd Ed., vol. 3, Academic Press, New York, 1998, pp. 136–146.
[22] G. Grynkiewicz, M. Poenie, R.Y. Tsien, A new generation of Ca^{2+} indicators with greatly improved fluorescence properties, J. Biol. Chem. 260 (1985) 3440–3450.
[23] G.A. Marguerie, T.S. Edgington, E.F. Plow, Interaction of fibrinogen with its platelet receptor as part of a multistep reaction in ADP-induced platelet aggregation, J. Biol.Chem. 255 (1980) 154–161.
[24] J.R. Lakowicz, Principles of Fluorescence Spectroscopy, Plenum Press, New York, 1999.
[25] M.P. Lillo, O. Cañadas, R.E. Dale, A.U. Acuña, Location and properties of the taxol binding center in microtubules: a picosecond laser study with fluorescent taxoids, Biochemistry 41 (2002) 12436–12439.
[26] J.M. Beechem, E. Gratton, M. Ameloot, J.R. Knutson, L. Brand, The global analysis of fluorescence intensity and anisotropy decay data, in: J.R. Lakowicz (Ed.), Second generation theory and programs, Topics in fluorescence spectroscopy, vol. 2, Plenum Press, NewYork, 1991, pp. 241–305.
[27] J.H. Brannon, D. Magde, Absolute quantum yield determination by thermal blooming. Fluorescein, J. Phys. Chem. 82 (1978) 705–709.
[28] M.P. Lillo, J.M. Beechem, B.K. Szpikowska, M.A. Sherman, M.T. Mas, Design and characterization of a multisite fluorescence energy-transfer system for protein folding studies: A steady-state and time-resolved study of yeast phosphoglycerate kinase, Biochemistry 36 (1997) 11261–11272.
[29] B.W. Van der Meer, G. Cooker, S.Y. Chen, Resonance Energy Transfer. Theory and data, VCH Publishers Inc., New York, 1994.
[30] J. Eisinger, J. Flores, Fluorometry of turbid and absorbant samples and the membrane fluidity of intact erythrocytes, Biophys. J. 48 (1985) 77–84.
[31] L.V. Parise, Integrin $\alpha_{IIb}\beta_3$ signaling in platelet adhesion and aggregation, Curr. Opin. Struct. Biol. 11 (1999) 597–601.
[32] C. Gachet, ADP receptors of platelets and their inhibition, Thromb. Haemost. 86 (2001) 222–232.
[33] S.R. Coughlin, How the protease thrombin talks to cells, Proc. Natl. Acad. Sci. U. S. A. 96 (1999) 11023–11027.
[34] R.V. Vassallo Jr, T. Kieber-Emmons, K. Cichowski, L.F. Brass, Structure-function relationships in the activation of the platelet thrombin receptors by receptor derived peptides, J. Biol. Chem. 267 (1992) 6081–6085.
[35] R. García-Guerra, J.A. García-Domínguez, J. González-Rodríguez, A new look at the lipid composition of the plasma membrane of human blood platelets relative to the GPIIb/IIIa (integrin $\alpha_{IIb}\beta_3$) content, Platelets 7 (1996) 195–205.
[36] W.I. Isenberg, R.P. McEver, D.R. Phillips, M.A. Shuman, D.F. Baiton, The platelet fibrinogen receptor: an immunogold-surface replica study of agonists-induced ligand binding and receptor clustering, J. Cell Biol. 104 (1987) 1655–1663.
[37] J. González-Rodríguez, A.U. Acuña, M.V. Alvarez, T.M. Jovin, Rotational mobility of the fibrinogen receptor glycoprotein IIb/IIIa or integrin $\alpha_{IIb}\beta_3$ in the plasma membrane of human platelets, Biochemistry 33 (1994) 266–274.
[38] C. Buensuceso, M. de Virgilio, S.J. Astil, Detection of integrin $\alpha_{IIb}\beta_3$ clustering in living cells, J.Biol.Chem. 278 (2003) 15217–15224.
[39] P.K. Wolber, B.S. Hudson, An analytical solution to the Foster energy transfer problem in two dimensions, Biophysical Journal 28 (1979) 197–210.
[40] P.J. Sims, M.H. Ginsberg, E.F. Plow, S.J. Shattil, Effect of platelet activation on the conformation of the plasma membrane glycoprotein IIb–IIIa complex, J. Biol. Chem. 266 (1991) 7345–7352.
[41] L. Mátyus, L. Bene, J. Harsfalvi, M.V. Alvarez, J. González-Rodríguez, A. Jenei, L. Muszbeck, S. Damjanovich, Organization of the glycoprotein (GP)IIb/IIIa heterodimer on resting human platelets studied by flow cytometric energy transfer, J. Photochem. Photobiol. B: Biol. 65 (2001) 47–58.
[42] A. Chigaev, G.J. Zwartz, T. Buranda, B.S. Edwards, E.R. Prossnitz, L.A. Sklar, Conformational regulation of α4β1-integrin affinity by reducing agents, J. Biol. Chem. 279 (2004) 32435–32443.